This is a preprint, the final version is subject to change, of the American Mineralogist (MSA)
Cite as Authors (Year) Title. American Mineralogist, in press.
(DOI will not work until issue is live.) DOI: http://dx.doi.org/10.2138/am.2014.4444

REVISION 2

Measurement of water contents in olivine using Raman spectroscopy

N. BOLFAN-CASANOVA[1], G. MONTAGNAC[2] ET B. REYNARD[2]

[1]Laboratoire Magmas et Volcans, Clermont-Ferrand

[2]Laboratoire de Sciences de la terre de l'ENS Lyon, Lyon

ABSTRACT

We have measured the water contents in forsterites and olivines synthesized in the multi-anvil press using confocal Raman spectroscopy. These samples were previously characterized for water contents by polarized FTIR and contain from 75 to 1300 ppm wt H_2O. We find that both forsterite and olivine follow the same trend in water content versus integrated Raman OH/Si intensity. In addition three synthetic enstatites also display a linear trend in water versus OH/Si integrated Raman intensity but with a different slope than for olivine, indicating that the calibration for measuring water by Raman is a matrix dependent. Three glasses of different compositions (two rhyolites and one basalt) and different water contents were also analysed. Comparison with the forsterites and olivines shows that the Raman cross-section of these glasses is very different and their intensities must be corrected by different factors. Therefore, in order to be able to use glasses as external calibrants, prior knowledge of their behavior compared to well-characterized NAM standards is necessary.

KEYWORDS: Raman spectroscopy, quantification, water content, olivine

REVISION 2

INTRODUCTION

In order to constrain the deep water cycle, the knowledge of the storage capacity of water in nominally anhydrous minerals (NAMs) of the mantle is a key issue e.g. (Bolfan-Casanova, 2005; Férot and Bolfan-Casanova, 2012, Tenner et al., 2012). This is tackled by studying hydroxyl abundances in natural samples on one hand, and by investigating experimentally the high-pressure and high-temperature solubility of the water component in NAMs. Compared to natural samples, high-pressure synthetic samples are smaller in size, which introduces a limitation on the accuracy of water content measurements because the techniques developed so far, such as Fourier Transform Infrared spectroscopy (FTIR, Libowitzky and Rossman, 1996; Kovacs et al., 2010; Asimow et al., 2006), Secondary Ion Mass Spectroscopy (SIMS, Aubaud et al., 2004; Demouchy et al., 2005), Elastic Recoil Detection Analysis (Bureau et al., 2009; Withers et al., 2012), and Proton-proton scattering (P-P, Maldener et al., 2003) provide a spatial resolution that is quite good but not always sufficient for polyminerallic samples. Among these techniques, infrared spectroscopy, being a site-specific technique, provides useful information about the different sites of protonation within the mineral structure, one pitfall being that sufficient thickness is necessary to detect small amounts of water and thus the grain size is a limiting factor (typically thicknesses of 50 to 100 µm are necessary, implying grain sizes of the same order). The beam size of SIMS or ERDA, which are bulk methods, is comparable to that of FTIR. SIMS is also very useful to measure water-rich samples, i.e. that are too absorbing for FTIR, as is the case of wadsleyite for example (Demouchy et al., 2005; Bolfan-Casanova et al., 2012), and has in addition achieved quite low detection limits down to 50 ppm wt H_2O (see Koga et al., 2003; Mosenfelder et al., 2011). A limitation of the method is that it relies on external calibrants with a significant matrix effect (Koga et al., 2003; Mosenfelder et al., 2011). Both SIMS, ERDA or P-P

techniques have recently been used to calibrate the infrared absorption coefficients of the Mg_2SiO_4 polymorphs (Withers et al., 2012, for olivine, Deon et al., 2010, for wadsleyite; Koch-Muller and Rhede, 2010, for ringwoodite). Especially ERDA and P-P are calibration-free methods.

In the past we have used FTIR to analyze samples that were synthesized in chemically simple systems such as $MgO\text{-}SiO_2\text{-}H_2O$, $MgO\text{-}FeO\text{-}SiO_2\text{-}H_2O$ and $MgO\text{-}FeO\text{-}Al_2O_3\text{-}SiO_2\text{-}H_2O$, and with relatively high bulk water contents from 5 to 1 wt% H_2O. In these cases grain sizes are relatively large and allow absorbance techniques such as FTIR. However, if the peridotite system is to be studied, and also with lower water contents that are more realistic for the mantle, grain sizes may be reduced and the spatial resolution becomes an important issue to measure water contents. Using Raman spectroscopy beam sizes of 1x3 µm can be achieved (see Thomas et al; 2009) competing with the diffraction limit of infrared spectroscopy.

In the recent years, Raman spectroscopy has been developed to measure water in glasses (Thomas, 2000; Di Muro et al., 2006; Thomas et al., 2008) and has also been used to calibrate the water content in garnets (Thomas et al., 2008) down to 50 ppm wt H_2O. In this study we report for the first time Raman spectra of OH in olivine and apply for the first time Raman spectroscopy for the analysis of water in olivine. We measured both iron-free (forsterite end-member Mg_2SiO_4) and iron-bearing olivine $(Mg,Fe)_2SiO_4$. We also present preliminary data for enstatite, showing that the method can be extended to any NAM.

EXPERIMENTAL AND ANALYTICAL TECHNIQUES

Samples

REVISION 2

The samples from this study are doubly polished thin sections of high-pressure synthetic samples. These were synthesized in a multi-anvil press at Laboratoire Magmas et Volcans by Bali et al. (2008) in the MgO-SiO_2-H_2O system and by Férot and Bolfan-Casanova (2012) in the MgO-FeO-SiO_2-H_2O and MgO-FeO-Al_2O_3-SiO_2-H_2O systems, see **Table 1**. Three glasses were also analyzed: two natural rhyolites and one synthetic basalt (see compositions in **Table 2**) to test the external calibration method (see Thomas et al., 2008).

Infrared spectroscopy

Polarized and unpolarized Fourier Transform infrared spectra were acquired using a Vertex70 Bruker spectrometer coupled to a Hyperion microscope equipped with x15 objective and condenser at Laboratoire Magmas et Volcans (Clermont-Ferrand). In order to confine the measurement spot, the size of the aperture was varied from 30 to 50 µm. The spectra were measured through a CaF_2 plate with a resolution of 2 cm^{-1} and with up to 2000 scans. The spectra were integrated from 4000 to 3000 cm^{-1} and OH content quantified using the Beer-Lambert law. In previous studies (Bali et al., 2008; Férot. and Bolfan-Casanova , 2012), we used the Bell et al. (2003) extinction coefficient of 28450 l.mole H_2O^{-1}.cm^{-2}. However, Withers et al. (2012) reported new measurements of a suite of olivines synthesized at high-pressures using ERDA. They find a new extinction coefficient of 45200 l.mole H_2O^{-1}.cm^{-2}, meaning that the values published by Férot and Bolfan-Casanova (2012) are overestimated and should be multiplied by a factor of 2/3. The olivines of Withers et al. (2012) display the same spectral characteristics as ours and thus their extinction coefficient should be the best suited for our samples. Thus in **Table 1**, we also display the water contents calculated using the extinction coefficient of Withers et al. (2012). In the following of the paper we will only use these values. For enstatite, we used the integrated molar absorption coefficient of 80600

REVISION 2

100 L.mol^{-1}.cm^{-2} (Bell et al., 1995). We used the Beer-Lambert law to calculate the water contents
101 from measured absorbances:

102 $$C(ppm\ wt\ H_2O) = \frac{A}{\varepsilon\, t}\,.\,X \qquad (1)$$

103 where C is the concentration (ppm wt H_2O), A is the absorbance, ε is the extinction coefficient
104 (l.mole H_2O^{-1}.cm^{-2}), t is the thickness (cm) and X is the density factor. Density factors of 5358
105 and 5448 l.moles H_2O^{-1} were used for olivine and orthopyroxene respectively to convert water
106 contents from moles H_2O.l^{-1} into ppm wt H_2O, using the formula C (ppm wt H_2O)=C (mol
107 H_2O/l).X with X=18.10^6/ρ and ρ the density of the phase (g/cm^3). We used the densities from
108 the literature (olivine: Fisher and Medaris, 1969; pyroxene: Chai et al., 1997; HughJones and
109 Angel, 1997).

110 Quantitative OH contents were measured using polarized measurements on randomly
111 oriented crystals. Two polarized spectra were acquired for each crystal at 0 and 90° of the
112 extinction position as determined under crossed polars. Five grains of the same phase were
113 analyzed and generally yield good statistics. The orientation of the spectra were determined
114 based on the comparison of the silicate overtone bands of the sample with those of H_2O-free
115 single crystals cut and polished parallel to the three crystallographic axes. For forsterite we
116 used directly the method of Asimow et al. (2006) to recalculate the OH spectra parallel to the
117 principal crystallographic axes and then use these spectra to quantify the absolute water
118 contents by calculating the Total absorbance = A_a+A_b+A_c, where A_i are the absorbances
119 parallel to the principal axes (see Libowitsky and Rossman, 1996). However, for olivine, the
120 difference in composition between our olivines and San Carlos olivine used as the reference
121 for the principal axes overtone spectra, leads to spectral differences in the overtone region that
122 does not allow for recalculation of the OH spectra along the principal axes. In such cases, we
123 found grains that displayed orientations close to the principal directions (see Férot and
124 Bolfan-Casanova, 2012, for more details). This method yielded a maximum error of 20% that

was calculated as the relative difference in integrated intensity between the overtone spectra of the unknown sample and the overtone spectra of the oriented standard (see Férot and Bolfan-Casanova, 2012). The polarized FTIR spectra of forsterite and olivine are shown in **Figure 1**. The determination of water contents in forsterite, olivine and pyroxene using polarized infrared measurements were compared to the average of unpolarized measurements (10 acquisitions on 10 separate grains). The average unpolarized absorbance of randomly oriented grains is equal to one third of the total absorbance (Kovacs et al., 2008) see **Figure 2**.

Raman spectroscopy

We used a LabRam HR800 spectrometer from Jobin-Yvon equipped with a motorized XY stage, an Olympus confocal microscope with a long distance 100x objective at Laboratoire des Sciences de la Terre de l'Ecole Normale Supérieure de Lyon. In order to maximize the intensity of the beam we used a grating with 600 grooves/mm and excitation wavelength was 514.532 nm. The spectra were recorded using the Labspec Software from 100 to 1500 cm^{-1} and 2800 to 4000 cm^{-1} by using a Peltier-cooled CCD detector. The laser power was varied from 50 to 240 mW on the first series of measurements on forsterite. For subsequent measurements the power used was kept at 50 or 70 mW. The laser beam was focused on the sample by monitoring the maximum intensity of the most intense silicate vibration band below 1000 cm^{-1}. Because Raman scattering is polarized we analyzed several grains using an half-wave plate in order to obtain an average spectrum of the silicate and of the OH regions. Firstly, the spectrum of the silicate region was collected with 0.5 to 5 s collection time (see **Figure 3** for olivine and enstatite). The Raman spectrum of the forsterite in the silicate region is similar to that of olivine. In general, no baseline correction was needed for the silicate region. Then, the OH-region was measured with an acquisition time of 1 to 200 seconds. We

observed that the forsterites display a very steep fluorescence background (see **Figure 4,** due to trace amounts of Cr^{3+} incorporated during synthesis, originating from the $LaCrO_3$ furnace probably), while the olivines display an almost flat background. The reason why forsterite is contaminated by Cr from the furnace and not olivine is that the forsterite samples were synthesized in Pt capsules while olivine samples were synthesized in double capsules (outer Platinum capsule/inner Rhenium capsule). The rhenium wall apparently avoids the Cr contamination, while Pt alone does not.

After acquisition, the OH spectra of the minerals were corrected for a linear baseline using PeakFit Package Software (Jandel Scientific) and the area under the OH peaks was integrated using Kaleidagraph. The integrated intensities of both OH and silicate regions were normalized to 1 second and 1 mW. In order to correct for random fluctuations in intensity, the integrated OH intensity was normalized to the integrated intensity of the silicate region from 200 to 1000 cm^{-1}, and then averaged over all grains from one sample. This defines the OH/Si integrated intensity ratio as introduced by Arredondo and Rossman (2002). The details of the measurements are shown in **Table 3**. The error in OH/Si due to baseline correction is most of the time within 15% except for the water-poor samples, with a low signal to noise ratio, and for which the error estimated from repeated baseline corrections increases to 50%. The reproducibility of the measurements on olivine was calculated on the basis of two different series of measurements performed at different laser power, see **Table 3**. When the laser power was similar, 50 and 70 mW, the difference between the values of OH/Si does not exceed 11%. The difference increases to 30% when the power varies from 70 to 140 mW. Concerning forsterite we can not consider the reproducibility as the variations in power between the different series of measurements were too large (from 240, to 140 to 50 mW).

We also measured an oriented single crystal of San Carlos olivine along the principal directions, and used the polarized spectra in the silicate region to evaluate the degree of mis-

orientation of the final averaged spectra of the olivine unknown samples to analyze. The comparison was performed in the region of major intensity, i.e. between 760 and 900 cm^{-1}. The relative difference between the integrated intensity of the unknowns and that of the standard did not exceeded 25%.

The spectra of the glasses are shown in **Figure 5**. We used a baseline so that the correction was linear under the low-frequency (LF), high-frequency (HF) and water bands. Concerning Basalt#19, that was repeatedly analysed throughout the Raman session, the average of the integrated water band for this glass is of 162 ± 21 cps/mW that is a variability of 13 %.

RESULTS

Raman spectra of the forsterites and the olivines in the OH region after baseline correction are shown in **Figure 6 and 7**. For forsterite, the Raman spectra display the same bands as observed in the FTIR spectra at 3613, 3580, 3550, 3480, 3440 and 3150 cm^{-1}. The latter band is important only in forsterite hydrothermally annealed at pressures of 2.5 GPa. In the case of olivine, the Raman spectra also display bands at 3612, 3599, 3578, 3565, 3544, 3475 and 3352 cm^{-1}. The main difference between Raman and FTIR spectra is that the band at 3613 cm^{-1} has a weak Raman intensity compared to the other bands, the band at 3580 cm^{-1} being the most intense both in forsterites and olivines.

We note a good sensitivity to water content, and a very similar OH/Si ratio of olivine samples 964 and 1033 that contain 580 ± 100 and 550 ± 175, respectively, as determined by FTIR (see also the similar averaged spectrum in **Figure 7**).

The Raman spectra in the OH region of orthopyroxene 1033 (Al-free, containing 600 ppm wt H_2O) and 964 (Al-bearing, containing 890 ppm wt H_2O) display bands at 3672, 3652,

REVISION 2

3598, 3371 and 3495 cm^{-1}, as shown in **Figure 8**, similarly as observed in the FTIR spectra (see Férot and Bolfan-Casanova, 2012). The spectrum of the Al-bearing sample also displays a broader band around 3400 cm^{-1} compared to the Al-free sample, in agreement with the FTIR analysis.

Effect of measurement duration

We performed a test of the effect of the beam on the OH intensity of the most hydrous forsterite (#691). After measuring successive spectra of 10 seconds each at 70 mW we note no difference in OH intensity between the six successive spectra, or with the additional spectrum on the same spot but for 60 additional seconds.

Effect of water content on the silicate band region

We note that the integrated intensity of the silicate region decreases with increasing water content as shown in **Figure 9**. This phenomenon can readily be observed in the Raman spectra of hydrous wadsleyite published in the literature, which usually deteriorate with important band broadening (see for example Frost et al., 1999).

Effect of laser power

Table 3 shows that with increasing laser power from 50 to 240 mW the integrated intensity of the silicate bands and of the OH bands decreases. This is surprising since increasing laser power is expected to increase sampled volume, and hence, Raman intensity. The decrease of Raman bands intensity with increasing laser power could be explained by a self-absorption phenomenon that varies in magnitude with laser power. The net effect on the ratio of OH/Si integrated intensity is that it decreases with increasing laser power. Finally, the effect of laser power on the relationship between water content and OH/Si integrated Raman intensities is

that the slope decreases with decreasing laser power. This demonstrates that in order to quantify the concentration of species using Raman spectroscopy by comparison with the intensity of a reference material, the same laser power should be used.

The relationship between water content, as determined using polarised FTIR and the Raman OH/Si integrated intensity ratio is displayed in **Figure 10A**. Using this representation, forsterite and olivine both display a linear response and align on the same trend. Also enstatite displays a linear response but with a different slope. **Figure 10B** displays the water content versus integrated OH Raman intensity relationship for forsterite and olivine but also includes the measurements on the three glasses. We observe that only the ATHO glass falls within the trend defined by the forsterite and olivine data. The linear regression on the olivine data in **Figure 10B** was used to correct the integrated OH intensity of the three glasses knowing their water contents. This allows estimating the correction factors for the three glasses (1.76 for ATHO, 2.4 for Güney Dag, 1.7 for Basalt#19). These correction factors are necessary if such glasses are to be used as external calibrants. These factors include differences in densities between the glasses (see **Table 2**) and the olivine (3.2 g/cm^3), but also differences in absorptivity (see Arredondo and Rossman, 2002; Thomas et al., 2008; Mercier et al., 2009), which are difficult to calculate a priori.

DISCUSSION

This study demonstrates that Raman spectroscopy can be used to quantify the water content in olivine. The results show a linear relationship between water content determined from polarized IR and Raman OH/Si integrated intensity ratio. The quantification of water content in natural garnets with Raman spectroscopy has been examined previously (Arredondo and Rossman, 2002). Although a positive correlation between H_2O content and

REVISION 2

OH/Si ratio was observed, the correlation was not considered good enough, probably in relation with the differences in composition of the garnets. These authors examined a wide range of composition in the grossular and spessartine-almandine solid solutions, which could explain the variations in the water content versus OH/Si. Here, we observe no substantial matrix effect as the correlation of water as a function of OH/Si Raman integrated intensity is the same for forsterite and olivine (with composition varying from Fo 91.3±0.1 to 92.7±0.2, see Férot and Bolfan-Casanova, 2012). We believe that the water content versus OH/Si ratio working curve measured here can be used to quantify water in olivines within the range of mantle compositions. More complex variations in garnets are probably due to the complexity of their solid solutions in the natural samples used by Arredondo and Rossman (2002).

As thoroughly explained in the paper by Thomas et al. (2009), "a linear relationship exists between the measured Raman intensity and the concentration of activated species". Especially, the relationship between Raman intensity and concentration depends on the scattering cross-section and the excited volume (which includes the effect of density and refractive index). Thus, since the effect of laser power on the intensity is not linear, the measurements on the unknown samples and the standards should be performed under similar conditions of laser beam (laser power and microscope objectives).

In order to quantify OH contents in minerals with Raman spectroscopy, there are two possibilities: either to rely on the water content versus Raman OH/Si ratio and compare to well-known standards of the same mineral (**Figure 10a**) or rely on the water content versus OH integrated Raman intensity of a glass standard (**Figure 10b**). In the last case, the correction factor to apply to the intensity of the unknown samples must be known. Indeed, there is a strong matrix effect between glasses and nominally anhydrous minerals. This was treated by Thomas et al. (2008) by correcting for differences in refractive index and density between the glass standard and the minerals they studied, simply through a normalization procedure. This implies knowing the refractive index of our glass which is not the case. For

example, in the study of Thomas et al. (2009), they corrected the integrated Raman intensity for density variations between the glass reference material and the garnets $I_{i,sample,corr}=I_{i,sample,meas}\ x\ d_{ref}/d_{sample}$ (g/cm^3), with d_{ref}/d_{sample} = 0.59±0.04. However, this does not take into account for other possible matrix effects such as reflection/refraction, self-absorption, etc… Thus, we find that the best method to constrain the matrix effect, hence the correction factor to apply to the unknowns is to first compare the water-intensity (i.e. water concentration vs OH Raman intensity) response of the future reference glasses to a pre-established mineral calibration. In order to align glasses and olivine on the same line, the glasses must be corrected for factors of 1.4, 2.4 and 1.7 for ATHO, basalt#19 and Güney Dag, respectively. Such variation in correction factors expresses differences in density and optical properties between the three glasses (see also **Table 2**). Alternatively, if we want to use ATHO (containing 710 ppm wt H_2O) in order to measure water in unknown olivine a density correction factor of 0.75=d_{ref}/d_{sample} (d_{ref} = 2.4 g/cm^3 and $d_{olivine}$ =3.2 g/cm^3) must be applied to the integrated intensity of the unknown olivines.

By using Raman spectroscopy Thomas et al. (2008) have been able to quantify water in natural garnets and to detect down to 3 ppm wt H_2O by applying 1 W and 600 sec. conditions. In this study we measured concentrations as low as 75 ppm wt H_2O in olivine (#955) by applying only 70 mW. Also, this work shows how useful Raman spectroscopy can be to analyze water contents in olivines from high-pressure experiments. The method is not as sensitive as FTIR but still water contents of 75 ppm wt H_2O are measurable in olivine. Preliminary data also show that the water content in enstatite can also be quantified by Raman, and thus this method could be extended to all sorts of mantle NAMs. This method should be very useful for analyzing water in small grain sized and polyphasic samples where FTIR or SIMS cannot be applied.

ACKNOWLEDGEMENTS

REVISION 2

Nathalie Bolfan-Casanova warmly thanks Etienne Médard and Nicolas Cluzel for providing the glass samples. This study was supported by INSU DieTY Program to Nathalie Bolfan-Casanova. This is Laboratory of Excellence *ClerVolc* contribution n°68.

REFERENCES CITED

Arredondo, E.H., and Rossman, G.R. (2002) Feasibility of determining the quantitative OH content of garnets with Raman spectroscopy. American Mineralogist, 87(2-3), 307-311.

Asimow, P.D., Stein, L.C., Mosenfelder, J.L., and Rossman, G.R. (2006) Quantitative polarized FTIR analysis of trace OH in populations of randomly oriented mineral grains. American Mineralogist(91), 278-284.

Aubaud, C., Hauri, E.H., and Hirschman, M.M. (2004) Hydrogen partition coefficients between nominally anhydrous minerals and basaltic melts. Geophysical Research Letters (31, L20611, doi:10.1029/2004GL021341.).

Bali, E., Bolfan-Casanova, N., and Koga, K.T. (2008) Pressure and temperature dependence of H solubility in forsterite: An implication to water activity in the Earth interior. Earth and Planetary Science Letters, 268(3-4), 354-363.

Bell, D.R., Ihingher, P.D., and Rossman, G.R. (1995) Quantitative analysis of trace OH in garnet and pyroxenes. American Mineralogist (80), 465-474.

Bolfan-Casanova, N. (2005) Water in the Earth's mantle. Mineralogical Magazine, 69, 227-255.

Bolfan-Casanova, N., Munoz, M., McCammon, C., Deloule, E., Ferot, A., Demouchy, S., France, L., Andrault, D., and Pascarelli, S. (2012) Ferric iron and water incorporation in wadsleyite under hydrous and oxidizing conditions: A XANES, Mossbauer, and SIMS study. American Mineralogist, 97(8-9), 1483-1493.

Bureau, H., Raepsaet, C., Khodja, H., Carraro, A., and Aubaud, C. (2009) Determination of hydrogen content in geological. Samples using elastic recoil detection analysis (ERDA). Geochimica Et Cosmochimica Acta, 73(11), 3311-3322.

Cluzel N., 2007, Simulation expérimentale de l'ascension et de la vésiculation des magmas rhyolitiques : Application à la cinétique de nucléation des bulles et implications volcanologiques, phD dissertation.

Demouchy, S., Deloule, E., Frost, D.J., and Keppler, H. (2005) Pressure and temperature dependence of water solubility in Fe-free wadsleyite. American Mineralogist(90), 1084-1091.

Deon, F., Koch-Muller, M., Rhede, D., Gottschalk, M., Wirth, R., and Thomas, S.M. (2010) Location and quantification of hydroxyl in wadsleyite: New insights. American Mineralogist, 95(2-3), 312-322.

Di Muro, A., Villemant, B., Montagnac, G., Scaillet, B., and Reynard, B. (2006) Quantification of water content and speciation in natural silicic glasses (phonolite, dacite, rhyolite) by confocal microRaman spectrometry. Geochimica Et Cosmochimica Acta, 70(11), 2868-2884.

Druitt, T.H., Brenchley, P.J., Gokten, Y.E., and Francaviglia, V. (1995) Late Quaternary Rhyolitic Eruptions from the Acigol Complex, Central Turkey. Journal of the Geological Society, 152, 655-667.

Férot, A., and Bolfan-Casanova, N. (2012) Water storage capacity in olivine and pyroxene to 14 GPa: Implications for the water content of the Earth's upper mantle and nature of seismic discontinuities. Earth and Planetary Science Letters, 349â€“350(0), 218-230.

Frost, D.J., and Fei, Y.W. (1998) Stability of phase D at high pressure and high temperature. Journal of Geophysical Research-Solid Earth, 103(B4), 7463-7474.

Jamtveit, B., Brooker, R., Brooks, K., Larsen, L.M., and Pedersen, T. (2001) The water content of olivines from the North Atlantic Volcanic Province. Earth and Planetary Science Letters, 186(3-4), 401-415.

Koch-Muller, M., and Rhede, D. (2010) IR absorption coefficients for water in nominally anhydrous high-pressure minerals. American Mineralogist, 95(5-6), 770-775.

Koga, K., Hauri, E., Hirschmann, M., and Bell, D. (2003) Hydrogen concentration analyses using SIMS and FTIR: comparison and calibration for nominally anhydrous minerals. Geochemistry Geophysics and Geosystems(4), 1019, doi:10.1029/2002GC000378.

Kovacs, I., Hermann, J., O'Neill, H.S.C., Gerald, J.F., Sambridge, M., and Horvath, G. (2008) Quantitative absorbance spectroscopy with unpolarized light: Part II. Experimental evaluation and development of a protocol for quantitative analysis of mineral IR spectra. American Mineralogist, 93(5-6), 765-778.

Kovacs, I., O'Neill, H.S.C., Hermann, J., and Hauri, E.H. (2010) Site-specific infrared O-H absorption coefficients for water substitution into olivine. American Mineralogist, 95(2-3), 292-299.

Lange, R.A. (1997) A revised model for the density and thermal expansivity of K2O-Na2O-CaO-MgO-Al2O3-SiO2 liquids from 700 to 1900 K: extension to crustal magmatic temperatures. Contributions to Mineralogy and Petrology, 130(1), 1-11.

Lange, R.A., and Carmichael, I.S.E. (1987) Densities of Na2o-K2o-Cao-Mgo-Feo-Fe2o3-Al2o3-Tio2-Sio2 Liquids - New Measurements and Derived Partial Molar Properties. Geochimica Et Cosmochimica Acta, 51(11), 2931-2946.

Lemaire, C., Kohn, S.C., and Brooker, R.A. (2004) The effect of silica activity on the incorporation mechanisms of water in synthetic forsterite: a polarised infrared spectroscopic study. Contribution to Mineralogy and Petrology(147), 48-57.

Libowitzky, E., and Rossman, G.R. (1996) Principles of quantitative absorbance measurements in anisotropic crystals. Physics and Chemistry of Minerals(23), 319-327.

Medard, E., and Grove, T.L. (2008) The effect of H2O on the olivine liquidus of basaltic melts: experiments and thermodynamic models. Contributions to Mineralogy and Petrology, 155(4), 417-432.

Mercier, M., Di Muro, A., Giordano, D., Metrich, N., Lesne, P., Pichavant, M., Scaillet, B., Clocchiatti, R., and Montagnac, G. (2009) Influence of glass polymerisation and oxidation on micro-Raman water analysis in alumino-silicate glasses. Geochimica Et Cosmochimica Acta, 73(1), 197-217.

Mosenfelder, J.L., Le Voyer, M., Rossman, G.R., Guan, Y.B., Bell, D.R., Asimow, P.D., and Eiler, J.M. (2011) Analysis of hydrogen in olivine by SIMS: Evaluation of standards and protocol. American Mineralogist, 96(11-12), 1725-1741.

Ochs, F.A., and Lange, R.A. (1997) The partial molar volume, thermal expansivity, and compressibility of H2O in NaAlSi3O8 liquid: new measurements and an internally consistent model. Contributions to Mineralogy and Petrology, 129(2-3), 155-165.

Tenner, T.J., Hirschmann, M.M., Withers, A.C., and Ardia, P. (2012) H2O storage capacity of olivine and low-Ca pyroxene from 10 to 13 GPa: consequences for dehydration melting above the transition zone. Contributions to Mineralogy and Petrology, 163(2), 297-316.

Thomas, R. (2000) Determination of water contents of granite melt inclusions by confocal laser Raman microprobe spectroscopy. American Mineralogist, 85, 868–872.

Thomas, S.M., Thomas, R., Davidson, P., Reichart, P., Koch-Muller, M., and Dollinger, G. (2008) Application of Raman spectroscopy to quantify trace water concentrations in glasses and garnets. American Mineralogist, 93(10), 1550-1557.

Thomas, S.-M., Koch-Müller, M., Reichart, P., Rhede, D., Thomas, R., Wirth, R., Matsyuk, S. (2009) IR calibrations for water determination in Olivine, r-GeO_2 and SiO_2 polymorphs. Physics and Chemistry of Minerals, 36, 489-509.

Withers, A.C., Bureau, H., Raepsaet, C., and Hirschmann, M.M. (2012) Calibration of infrared spectroscopy by elastic recoil detection analysis of H in synthetic olivine. Chemical Geology, 334, 92-98.

REVISION 2

Figure captions

Figure 1 Polarized FTIR spectra of (A) forsterite samples from Bali et al. (2008), and (B) of olivine samples from Férot and Bolfan-Casanova (2012). Water contents shown are corrected following the extinction coefficient of Withers et al. (2012). Spectra shown are for different orientations and different water contents. The spectra of samples 556 and 923 were multiplied by 5.

Figure 2. Comparison between water concentrations calculated from the average of unpolarized spectra measured on several grains, then multiplied by three following Kovacs et al. (2008) and water concentrations measured using polarized radiation in olivine and enstatite in the MFSH and MFASH systems as measured using selected polarized spectra close to the principal directions from Férot and Bolfan-Casanova (2012) and in forsterite as determined using the method of Asimow et al. (2006) from Bali et al. (2008).

Figure 3. Raman spectra of the silicate region of (**A**) olivine 955 and (**B**) orthopyroxene 964. The bold curve corresponds to the average of all spectra. Virtually no baseline correction was necessary.

Figure 4. Raman spectra of the driest sample used in this study: forsterite 556 containing 75 ppm wt H_2O, measured for 20 seconds using 140 mW.

Figure 5. Main Raman bands of the glasses (red curve is ATHO, green curve for Basalt #19 and blue curve for Güney Dag).

REVISION 2

Figure 6. Raman spectra of the forsterites in the OH region, recorded at the same power of 240 mW. The spectra measured on several grains are shown and give a representation of the extent of anisotropy sampled. The intensity of the spectra of sample 556 was multiplied by 10 for clarity. Thick curve represents the average spectrum.

Figure 7. A) Raman spectra of olivines in the OH region. For clarity, only the final total absorbance spectra are shown, which are derived from averaging several measurements on different grains. The intensity of the spectrum of sample 955 is multiplied by 5, also for clarity. B) Raman spectra of olivine 949 measured along different orientations (the thick curve corresponds to the average of all spectra).

Figure 8. Raman spectra of enstatites in the OH region. For clarity, only the averaged spectra are shown. Sample 964 displays a high and broad band at 3495 cm^{-1} which is due to the presence of Al (in contrast to samples 949 and 1033 that were synthesized in an Al-free system).

Figure 9. Effect of water content on the integrated Raman intensity of the silicate region. Wadsleyite from (Bolfan-Casanova, unpublished).

Figure 10. (**A**) Correlation between water content in forsterite and olivine and the integrated OH/Si Raman intensity. Also shown is the trend for enstatite. (**B**) Correlation between water content and the integrated OH Raman intensity of olivine and of the glasses and the corrected glasses.

Table 1a. Water content of the olivine samples

Sample	Water content (ppm wt H_2O)[3]		Composition (Fo content)[5]
	Bell et al. (2003)	Withers et al. (2012)	
Forsterite[1]			
556	111 ± 11	74 ± 7	100
559	607 ± 61	405 ± 40	100
691	1189 ± 119	793 ± 80	100
Olivine[2]			
955	126 ± 11	84 ± 7	92.6 ± 0.2
923 [4]	184 ± 52	123 ± 35	91.9 ± 0.5
964 [4]	876 ± 147	584 ± 98	91.3 ± 0.1
949	2071 ± 461	1381 ± 307	92.7 ± 0.2
1033	830 ± 260	553 ± 173	92.7 ± 0.2

[1] see Bali et al. (2008) for details
[2] see Férot and Bolfan-Casanova (2012) for details
[3] Water contents calculated using the extinction coefficient of 28,450 $L.mol^{-1}.cm^{-2}$ from Bell et al. (2003) or 45,200 $L.mol^{-1}.cm^{-2}$ from Withers et al. (2012).
[4] Samples synthesized in the MFASH system and thus containing trace amounts of aluminum.
[5] Forsterite content = 100 x $X_{Mg}/(X_{Mg}+X_{Fe})$, with X being the molar concentration

Table 1b. Water content of the clinoenstatite samples

Sample	Water content (ppm wt H_2O)[1]	Composition (Fe content)[2]
949	1331 ± 138	92.7 ± 0.2
964	884 ± 147	92.8 ± 0.2 [3]
1033	593 ± 214	92.7 ± 0.2

[1] Water contents calculated using the extinction coefficient of Bell et al. (1995).
[2] Ferrosilite content = 100 x $X_{Mg}/(X_{Mg}+X_{Fe})$, with X being the molar concentration.
[3] Sample synthesized in the MFASH system and containing 0.006 Al per formula unit.

Table 2. Composition of the glasses analyzed

Oxides (wt%)	ATHO [1]	Basalt#19 [2]	Güney Dag [3]
SiO_2	74.97 (0.44)	47.3 (5)	76.51
Al_2O_3	11.86 (0.57)	18.6 (2)	12.56
FeO	3.66 (0.11)	8.57 (3)	0.78
MgO	0.10 (0.03)	10.6 (2)	0.01
CaO	1.61 (0.17)	11.73 (13)	0.25
Na_2O	4.20 (0.20)	2.24 (11)	4.47
K_2O	2.54 (0.08)	0.07 (3)	4.24
TiO_2	0.24 (0.01)	0.57 (6)	0.03
MnO	0.10 (0.00)	0.15 (2)	0.07
P_2O_5	0.03 (0.02)	0.06 (2)	n.d.
Total	99.30	98.05	98.92
H_2O content (wt%)	0.071	0.44	1.10
Densities (g/cm^3)[4]	2.4	2.8	2.3

sources : [1] : Druitt et al. (1995) ; [2] : Médard and Grove (2008) ; [3] : Olgeir Sigmarsson, *pers. comm.* All water contents measured by FTIR and those of ATHO and Güney Dag by Cluzel (2007). 4: densities calculated form the data of Lange (1997), Lange and Carmichael (1987) and Ochs and Lange (1997).

Table 3. Results of the Raman measurements. Only the data in bold were used in Figure 10.

Mineral	Sample	Water content (ppm wt H_2O)	I_{OH}	I_{Si}	OH/Si [1]	n	laser power (mW)
Forsterite	**556**	**74 ± 7**	3.5 ± 0.9	7310 ± 200	4.8E-04 ± 1.4E-04	3	240
			7.7 ± 2.9	**8297 ± 594**	**9.3E-04 ± 3.8E-04**	**7**	**140**
	559	**405 ± 40**	17 ± 11	7420 ± 408	2.3E-03 ± 1.4E-03	4	240
			44 ± 15	**9650 ± 938**	**4.6E-03 ± 1.3E-03**	**6**	**50**
	691	**793 ± 80**	64 ± 29	8413 ± 2097	7.6E-03 ± 3.8E-03	4	240
			84 ± 18	9684 ± 725	1.1E-02 ± 2.1E-03	5	50
			96 ± 34	**6840 ± 785**	**1.4E-02 ± 4.8E-03**	**12**	**70**
Olivine	**955**	**84 ± 7**	**0.6 ± 03**	**9024 ± 928**	**6.3E-05 ± 3.6E-05**	**10**	**70**
	923	**123 ± 35**	**2.8 ± 2.6**	**6877 ± 542**	**4.0E-04 ± 3.8E-04**	**6**	**215**
	964	**584 ± 98**	64 ± 39	6848 ± 568	9.3E-03 ± 6.5E-03	8	70
			47 ± 19	**4756 ± 825**	**1.0E-02 ± 4.5E-03**	**11**	**70**
	1033	**553 ± 173**	46 ± 8	5578 ± 632	8.2E-03 ± 2.1E-03	4	140
			60 ± 19	**5757 ± 425**	**1.0E-02 ± 3.5E-03**	**8**	**70**
	949	**1381 ± 307**	220 ± 68	9457 ± 546	2.3E-02 ± 7.6E-03	6	50
			117 ± 34	**5041 ± 642**	**2.3E-02 ± 7.0E-03**	**10**	**70**
Enstatite	**1033**	**593 ± 214**	**23 ± 3**	**5907 ± 804**	**4.0E-03 ± 9.6E-04**	**8**	**70**
	964	**884 ± 147**	**50 ± 27**	**5924 ± 1583**	**7.5E-03 ± 2.3E-03**	**9**	**70**
	949	**1331 ± 138**	**40 ± 11**	**4882 ± 1108**	**8.8E-03 ± 3.7E-03**	**6**	**70**
Glasses	**ATHO**	**710**	**44 ± 4**			**3**	**70**
	Basalt#19	**4400**	**162 ± 21**			**12**	**70**
	Güney Dag	**11000**	**581 ± 120**			**3**	**70**

[1] the standard deviation represents the anisotropy of absorption. The error due to mis-orientation of the average compared to an oriented single crystal of San Carlos olivine does not exceed 25 % (see text).

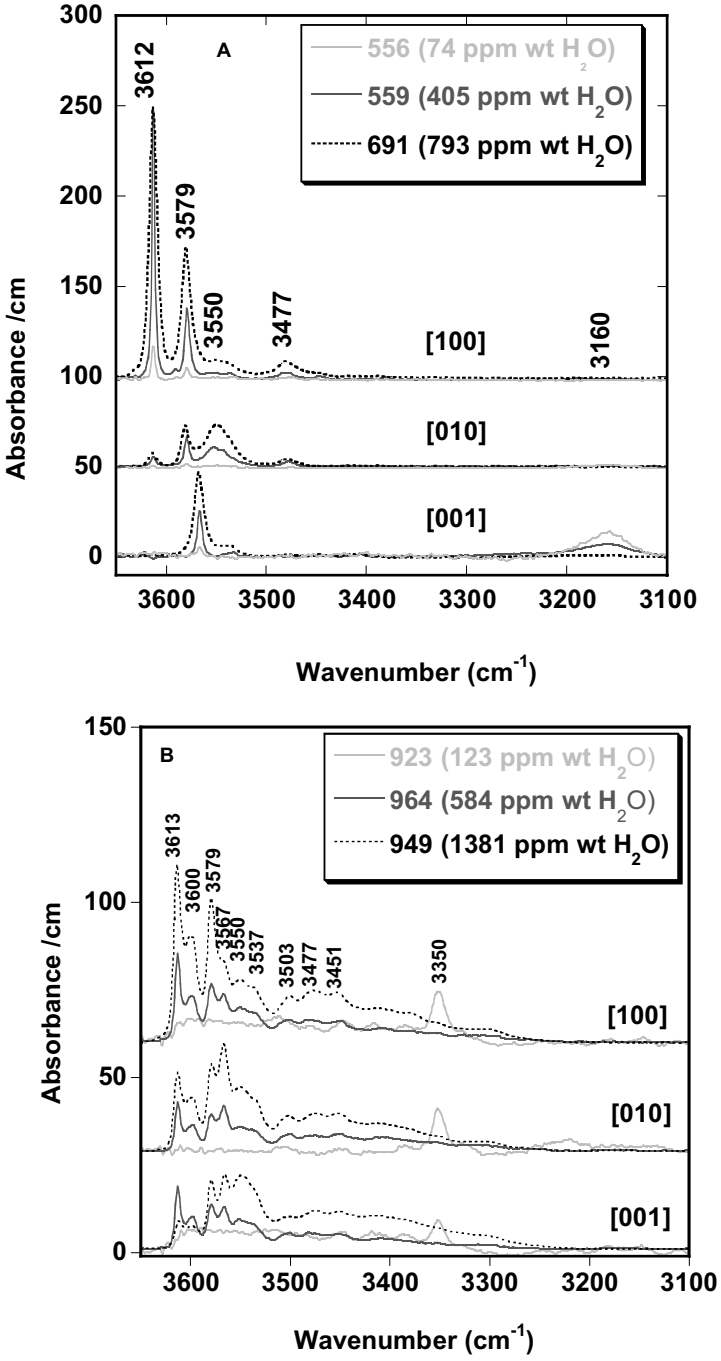

Figure 1

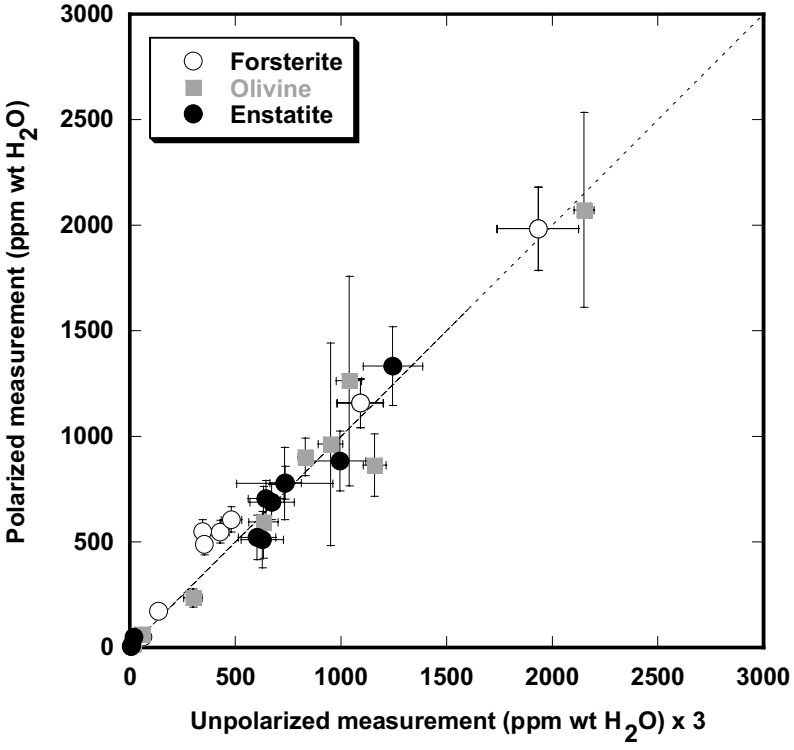

Figure 2

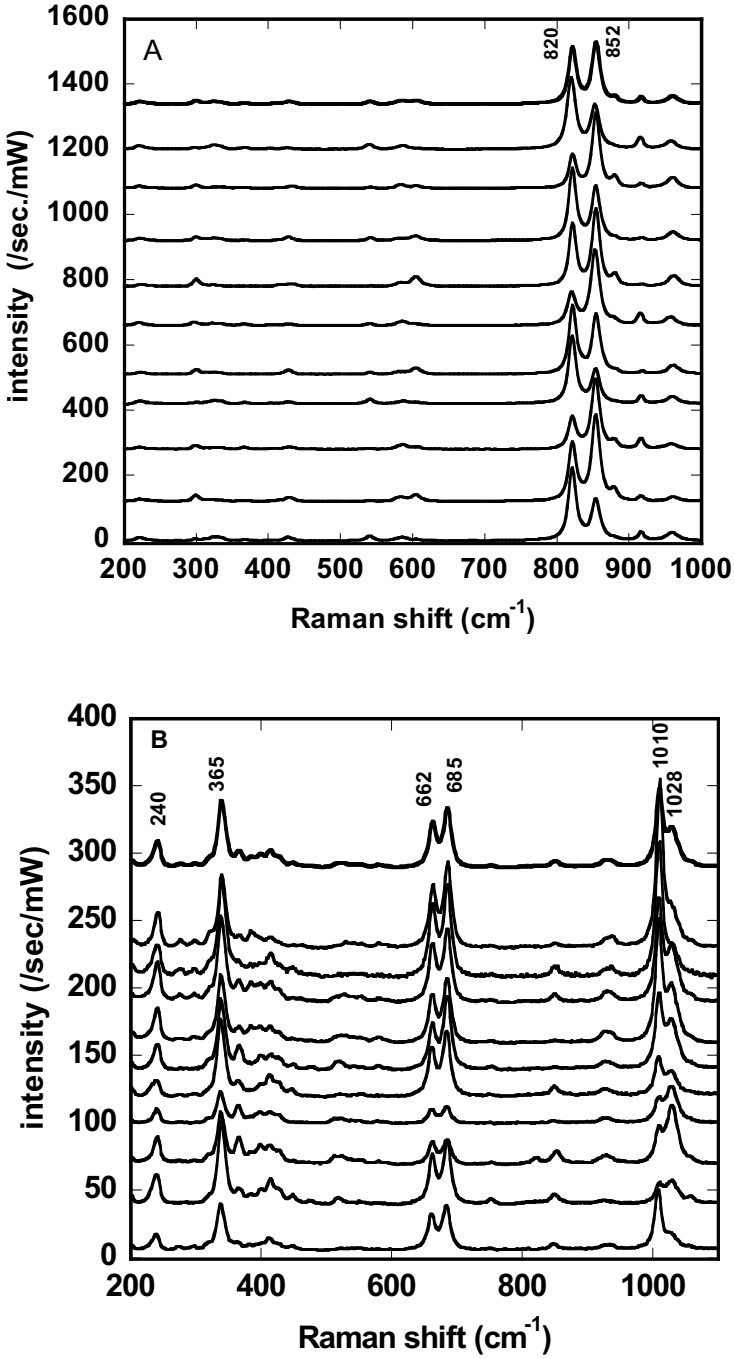

Figure 3

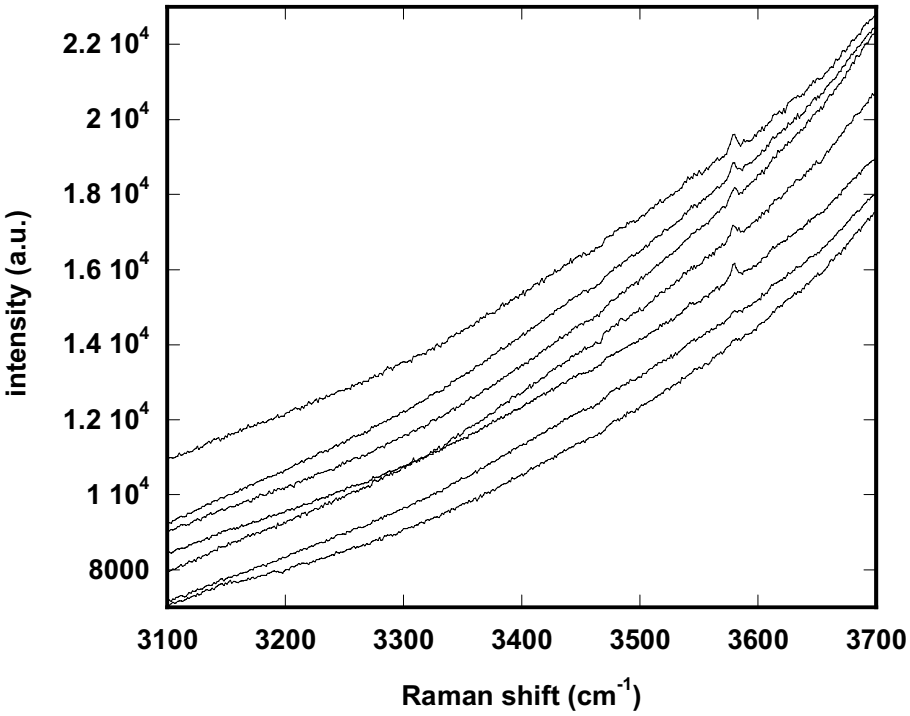

Figure 4.

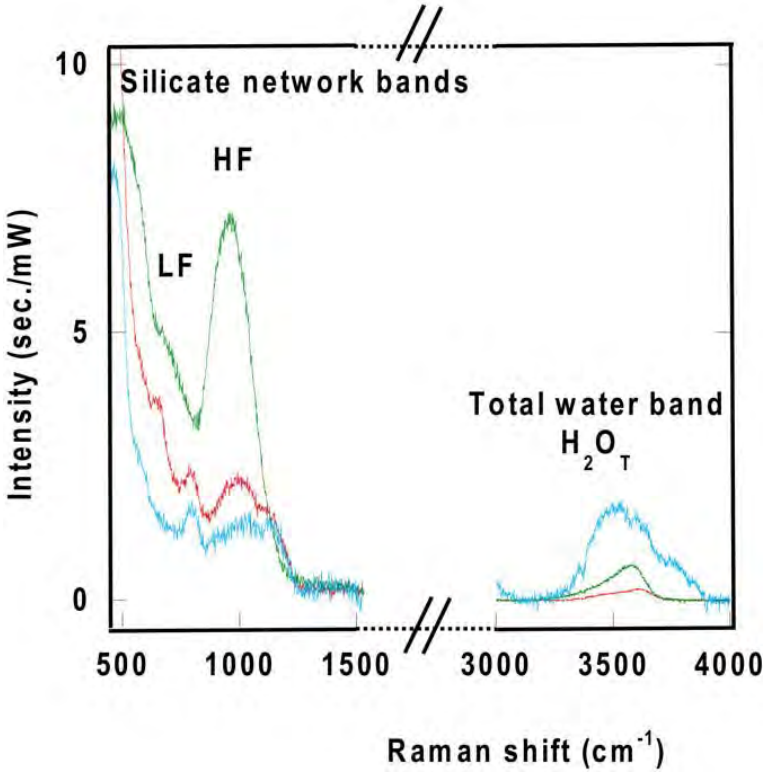

Figure 5.

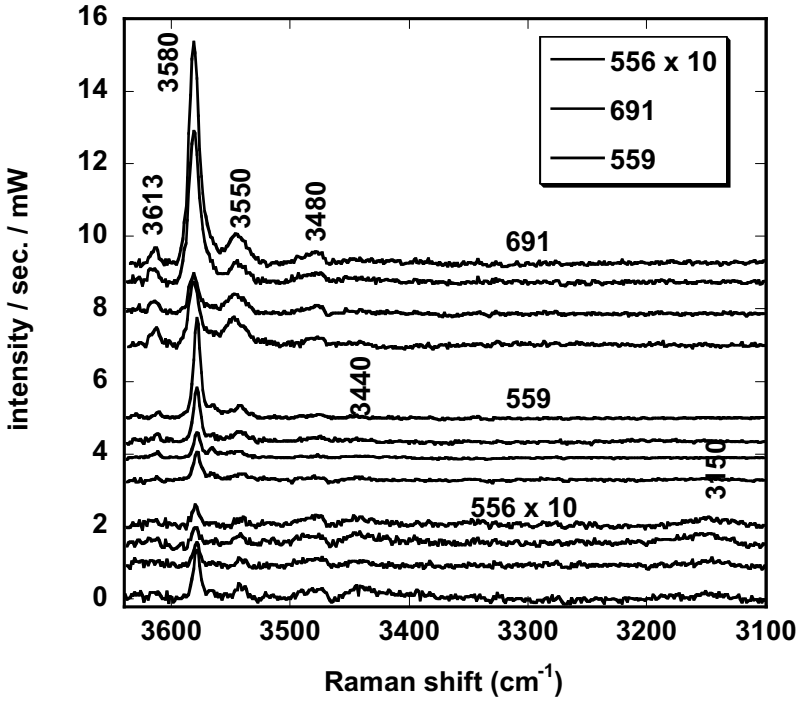

Figure 6.

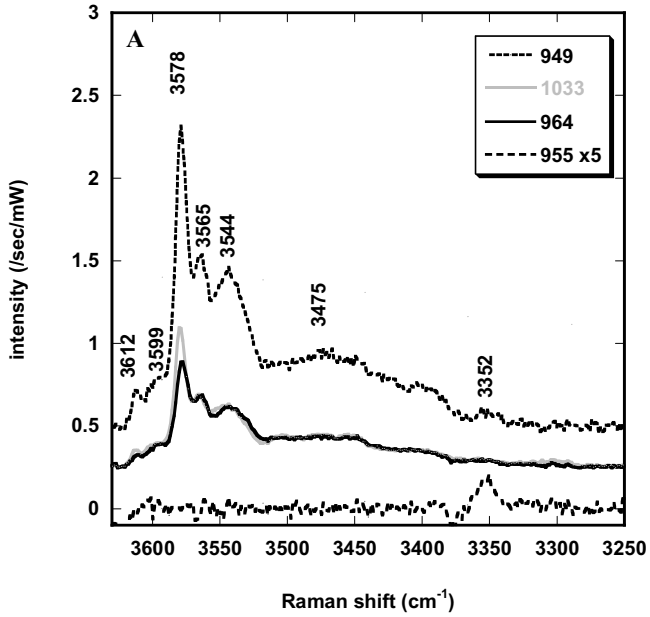

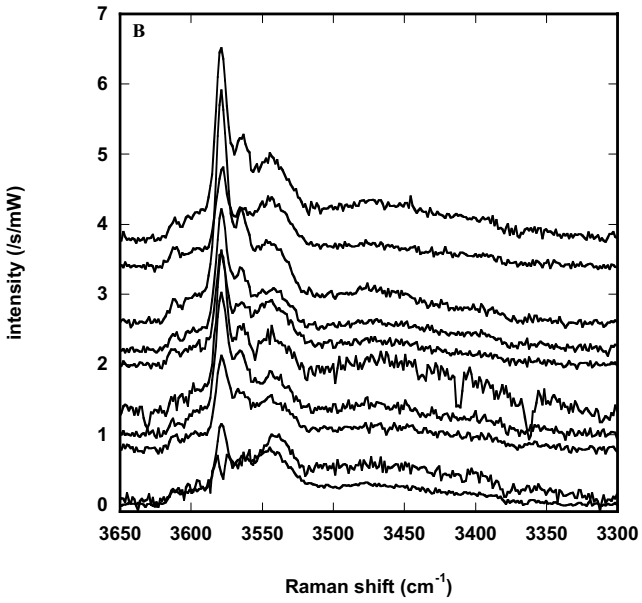

Figure 7

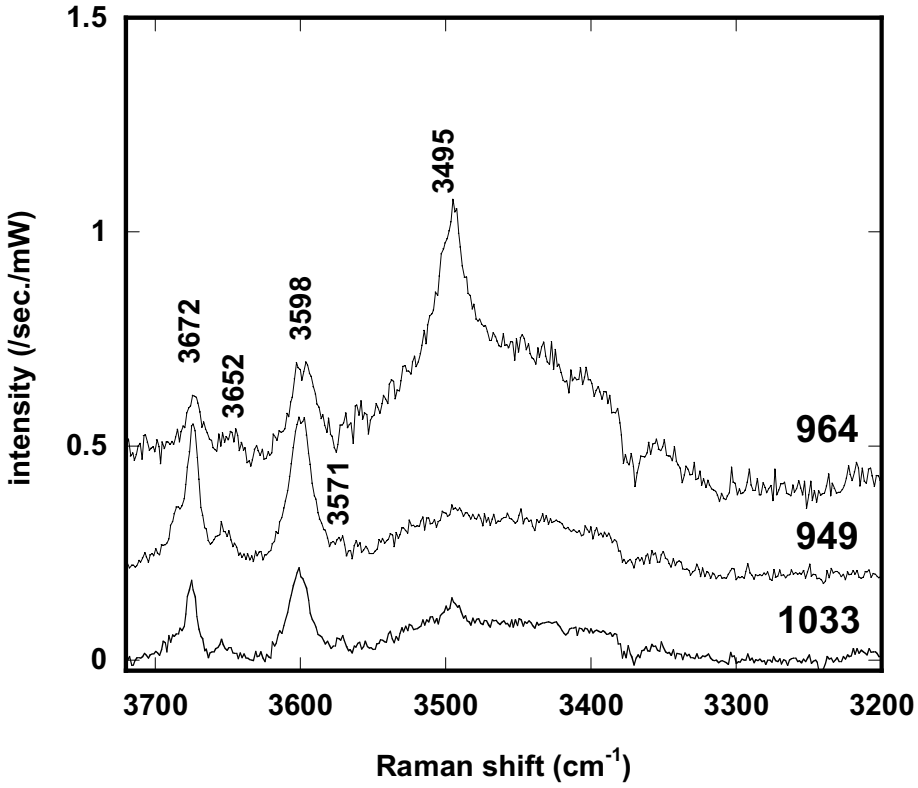

Figure 8.

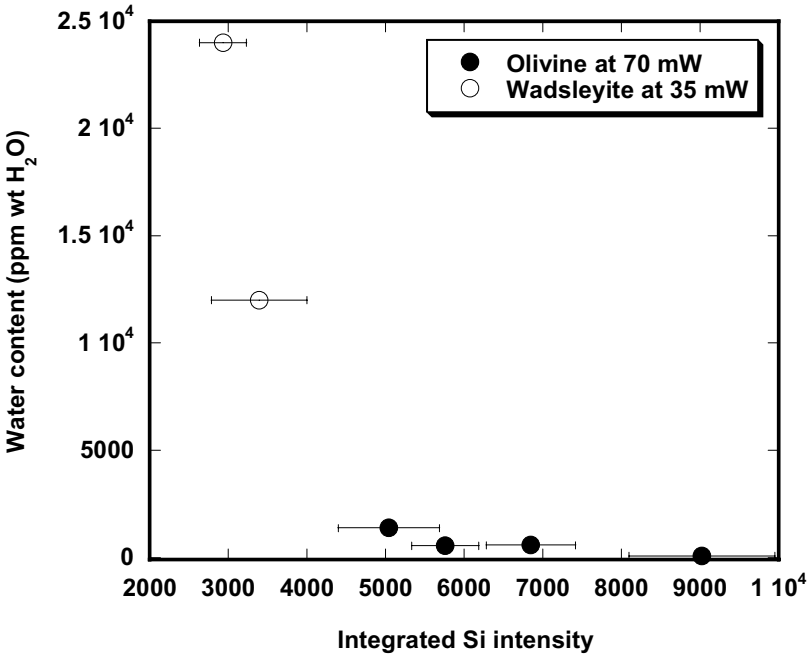

Figure 9

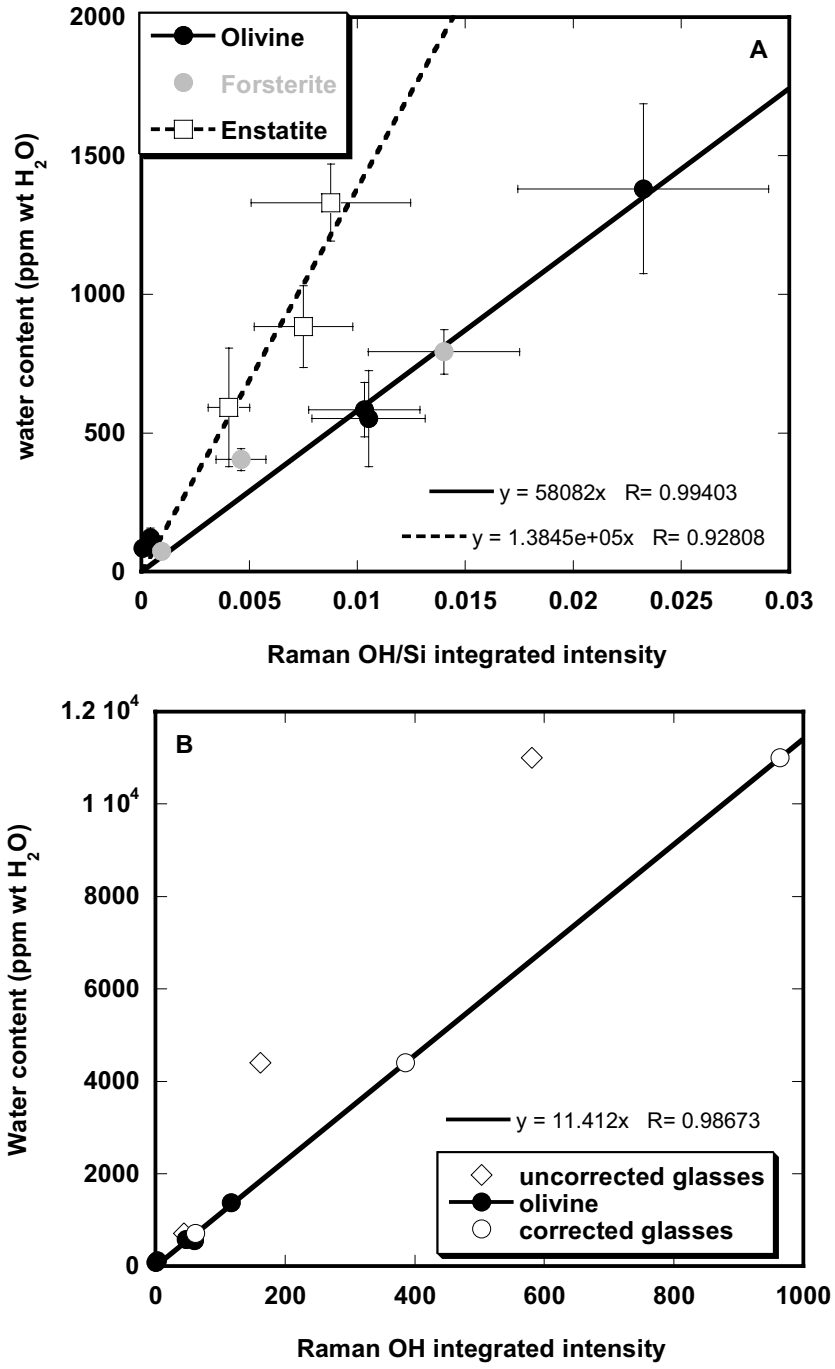

Figure 10.